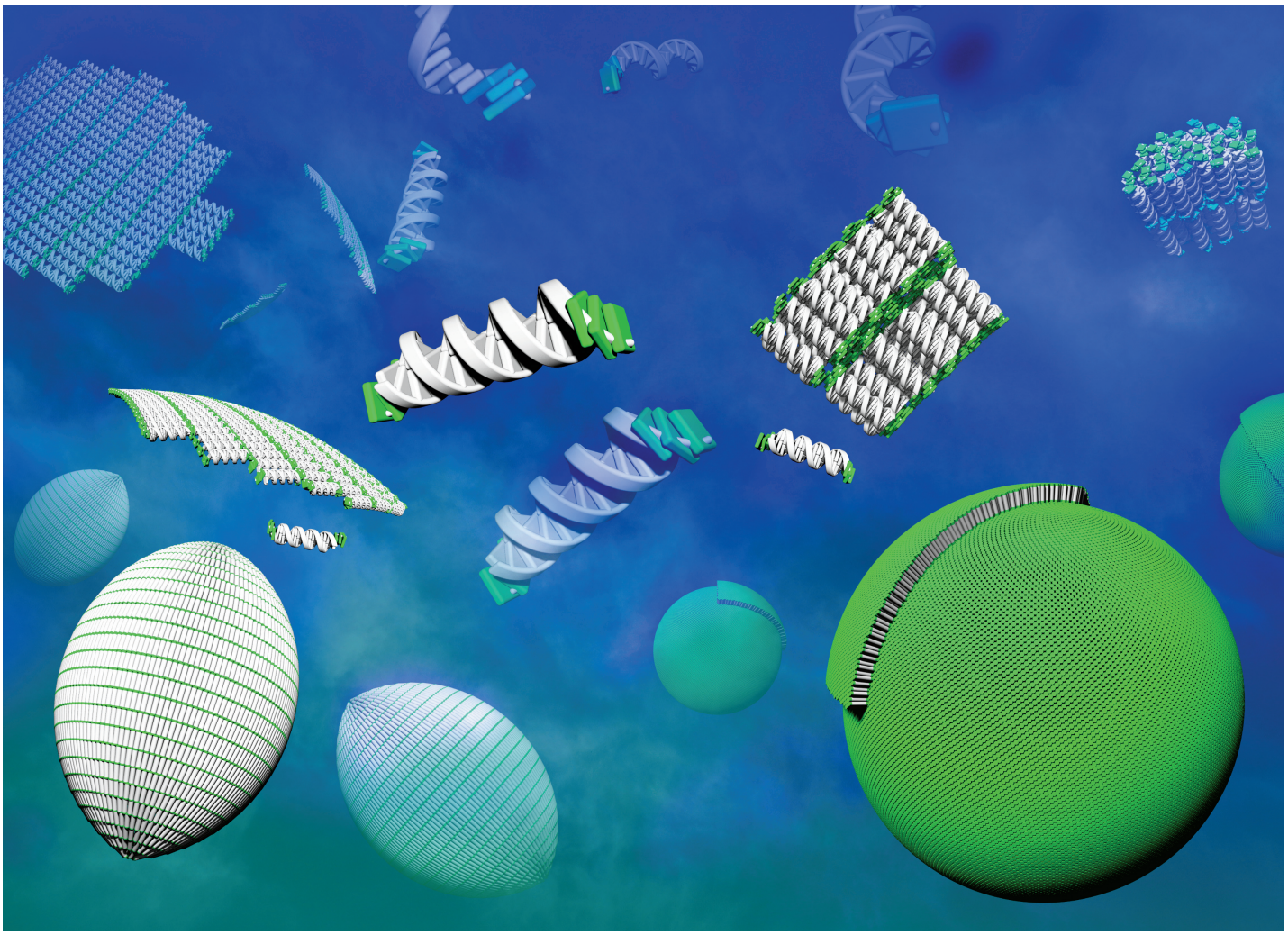

Showcasing research from the groups of Prof. Robert Häner and Prof. Benoît Zuber of the University of Bern, Switzerland.

Supramolecular assembly of DNA-constructed vesicles

Amphiphilic DNA hybrids self-assemble into two distinctly different types of vesicular architectures, in which DNA functions as the intrinsic structural element of the formed vesicles. As visualized by cryo-electron microscopy, the DNA hybrids can interact either in an extended or in a compact fashion. The two types of DNA packing result in divergent functional properties. In particular, the mode of packing affects the accessibility of the DNA, as demonstrated by light-harvesting and intercalation experiments.

As featured in:

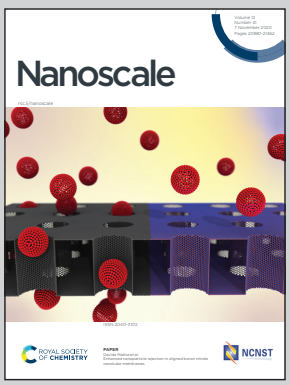

See Benoît Zuber, Robert Häner *et al.*, *Nanoscale*, 2020, **12**, 21118.

ROYAL SOCIETY OF CHEMISTRY

rsc.li/nanoscale

Registered charity number: 207890

Nanoscale

ROYAL SOCIETY OF CHEMISTRY

COMMUNICATION

View Article Online
View Journal | View Issue

Cite this: *Nanoscale*, 2020, **12**, 21118

Received 28th May 2020,
Accepted 28th June 2020

DOI: 10.1039/d0nr04103c

rsc.li/nanoscale

Supramolecular assembly of DNA-constructed vesicles†

Simon Rothenbühler, [a] Ioan Iacovache,[b] Simon M. Langenegger,[a] Benoît Zuber *[b] and Robert Häner *[a]

The self-assembly of DNA hybrids possessing tetraphenylethylene sticky ends at both sides into vesicular architectures in aqueous medium is demonstrated. Cryo-electron microscopy reveals the formation of different types of morphologies from the amphiphilic DNA-hybrids. Depending on the conditions, either an extended (sheet-like) or a compact (columnar) alignment of the DNA hybrids is observed. The different modes of DNA arrangement lead to the formation of vesicles appearing either as prolate ellipsoids (type I) or as spheres (type II). The type of packing has a significant effect on the accessibility of the DNA, as evidenced by intercalation and light-harvesting experiments. Only the vesicles exhibiting the sheet-like DNA alignment are accessible for intercalation by ethidium bromide or for the integration of chromophore-labelled DNA *via* a strand exchange process. The dynamic nature of type I vesicles enables their elaboration into artificial light-harvesting complexes by DNA-guided introduction of Cy3-acceptor chromophores. DNA-constructed vesicles of the kind shown here represent versatile intermediates that are amenable to further modification for tailored nanotechnology applications.

Introduction

DNA nanotechnology offers the possibility of a rational design and construction of precise architectures due to the reliability of nucleobase pairing.[1–4] The programmable bottom-up construction of nano-sized structures *via* DNA origami provides a variety of different shapes, such as rings, tubes, or polyhedra, among others.[5–7] Engineering short single-stranded overhangs, known as sticky ends, extend potential strategies for the assembly of DNA into nanostructures ranging from two-dimensional tiles, to three-dimensional DNA crystals, or nanocapsules.[8–12] Merging purely artificial DNA nucleotide surrogates with natural DNA nucleotides lead to DNA conjugates and the resulting functional supramolecular assemblies have recently gained much attention in the fields of nanotechnology and materials science.[13–19] Such functional supramolecular polymers feature properties beyond the classical role of DNA in biological systems, with applications in optoelectronic devices, drug delivery systems, and diagnostics to name a few.[20–28] However, vesicular morphologies are predominantly reported from lipid–DNA conjugates or DNA functionalized liposomes,[29–34] while the field apart from lipid-based DNA constructs remains largely unexplored.[35] In previous work, we demonstrated the self-assembly of phenanthrene–DNA conjugates into vesicular structures with light-harvesting features.[36] Combining this approach with the rapidly evolving area of aggregation-induced emission (AIE),[37–40] we herein present DNA constructs assembled from DNA conjugates, functionalized with the AIEgen tetraphenylethylene (TPE). The resulting AIE-active supramolecular assemblies were characterized by cryo-electron microscopy (cryo-EM)[41,42] at a resolution level of the width of a DNA duplex. Additionally, the accessibility of the DNA duplex within the two types of architectures was tested by DNA intercalation experiments using ethidium bromide (EthBr) and by light-harvesting experiments.

Results and discussion

The chemically modified oligonucleotides utilized in this work are depicted in Fig. 1. Strands **A** and **B** were prepared *via* solid-phase synthesis and are modified at their 3′-ends with three phosphodiester-linked *E*-TPE units. The synthesis of the corresponding TPE phosphoramidite building block was adapted from published procedures.[43] Due to the complementarity of DNA single strands **A** and **B**, they hybridize and form

[a]*Department of Chemistry and Biochemistry, University of Bern, Freiestrasse 3, CH – 3012 Bern, Switzerland. E-mail: robert.haener@dcb.unibe.ch; http://haener.dcb.unibe.ch*

[b]*Institute of Anatomy, University of Bern, Baltzerstrasse 2, CH – 3012 Bern, Switzerland. E-mail: benoit.zuber@ana.unibe.ch*

†Electronic supplementary information (ESI) available: Experimental procedures, NMR spectra, additional UV-vis and fluorescence spectra, additional cryo-EM images, AFM images, fluorescence quantum yield determination. See DOI: 10.1039/d0nr04103c

Strand	Sequence
A	5′-CAA GGT CCG ATG CAA GGA AG-(*E*-TPE)$_3$
B	(*E*-TPE)$_3$-GTT CCA GGC TAC GTT CCT TC-5′
C	5′-CAA GGT CCG ATG CAA GGA AG-3′
D	3′-GTT CCA GGC TAC GTT CCT TC-5′

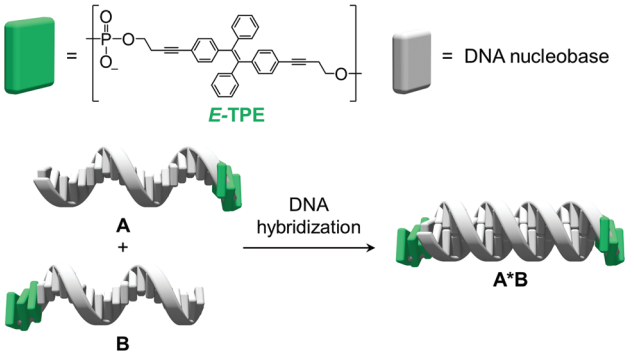

Fig. 1 Sequences of oligomers **A**–**D**, chemical structure of the TPE modification and illustration of DNA hybrid **A·B**.

the DNA duplex **A·B**, which contains TPE overhangs (sticky ends) on both sides.

Temperature dependent absorption profiles of **A·B** (Fig. 2) show a combination of absorption by TPE and the DNA nucleobases in the region around 260 nm (Fig. S13, ESI†). The structureless band around 330 nm, on the other hand, is due to TPE absorption only. The hypochromic effect of the 260 nm band upon controlled cooling from 75 °C to 20 °C originates from DNA hybridization. In addition, cooling of the solution results in a bathochromic shift of the maximum at 326 nm to 333 nm, due to TPE aggregation.

Cryo-EM enables the characterization of structures in their actual morphology, since vitrified specimens preserve the structures present in solution.[41,42] Therefore, the formation of supramolecular assemblies was investigated by cryo-EM (Fig. 3), which revealed the coexistence of two distinct morphologies. Hybrid **A·B** either self-assembles into vesicles with an extended alignment of the DNA duplexes (type I, Fig. 3, top)

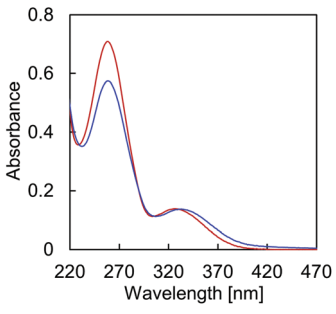

Fig. 2 Temperature-dependence of the absorption spectrum of hybrid **A·B**. Conditions: 1 μM **A·B**, 10 mM sodium phosphate buffer pH 7.2, 0.1 mM spermine·4 HCl, 20 vol% ethanol at 75 °C (red) and 20 °C after thermally controlled (0.5 °C min^{-1}) assembly process (blue).

or in a compact arrangement (type II, Fig. 3, bottom). More than 94% of all observed vesicles exhibit the rugby-ball-shaped morphology (type I) after assembly by a simple cooling procedure under these conditions. A notable feature of the extended architecture is the appearance of a regular pattern of discrete bands. The average distance between the bands is 7.8 ± 0.5 nm (Fig. 3 and Fig. S16, ESI†),[44–46] which corresponds well with the length of a 23-mer **A·B**, assuming a contact distance of 3.4 Å between base pairs or between stacked TPE units. The width of the DNA duplex **A·B** (see Fig. 3, inset) is also observable and found to be about 2.4 nm. The two morphologies exhibit different diameters: while the size range of type I vesicles is roughly between 50 and 100 nm, the diameter of type II vesicles ranges from 200 to 350 nm. A thickness of 10.9 ± 0.5 nm was observed for the membrane of the compact vesicles (Fig. 3, bottom), which agrees well with the length of hybrid **A·B**. The width of the DNA duplex **A·B** in type II vesicles was measured to be about 2.5 nm. In vesicles with this morphology, the TPE sticky ends are positioned on both sides of the membrane. Therefore, the assembly of additional layers of the same type is facilitated *via* π-stacking. As a result, double layers are clearly discernible in many areas of the images. The presence of spermine is essential for the assembly of the vesicles. DNA duplexes are tightly packed in both types of vesicles and the resulting coulombic repulsion between the negatively charged phosphate backbones is neutralized by the polycation. In the absence of spermine, no vesicles were visible by cryo-EM (Fig. S17, ESI†). The self-assembly of duplex **A·B** into vesicles is further affirmed by atomic force microscopy (AFM) images (Fig. S23, ESI†).

As described above, assembly of the vesicles from duplex **A·B** was accomplished in the presence of 20 vol% ethanol. In order to investigate the effect of solvent composition on the morphology, ethanol was removed by dialysis against 10 mM sodium phosphate buffer pH 7.2, containing 0.1 mM spermine·4 HCl. As evidenced by cryo-EM images (Fig. 4), the ratio of the two types of vesicles is substantially affected by dialysis. Whereas the vast majority of vesicles belonged to type I before dialysis, more than 90% exhibited the compact type II morphology (membrane thickness: 10.6 ± 0.6 nm) after removal of ethanol. Additionally, also the average diameter had decreased to 50–150 nm. Performing the thermally controlled assembly process in the absence of ethanol yielded only small, ill-defined aggregates (Fig. S20, ESI†). Thus, ethanol is required to assemble the vesicles in the first instance, which renders this two-step procedure necessary to obtain well-defined vesicles in the absence of ethanol.

Temperature-dependent fluorescence spectra (Fig. 5a) and fluorescence quantum yields (Φ_{FL}, Table 1) demonstrate the AIE properties of hybrid **A·B**. At 75 °C, emission is close to zero (Φ_{FL} < 0.75%) after TPE excitation at 335 nm. This suggests that the two single strands **A** and **B** are completely disassembled and that the TPE units show only negligible aggregation within the single stranded oligomers. In agreement with AIE properties, TPE fluorescence emerges during the assembly process (slowly cooling the solution to 20 °C). The

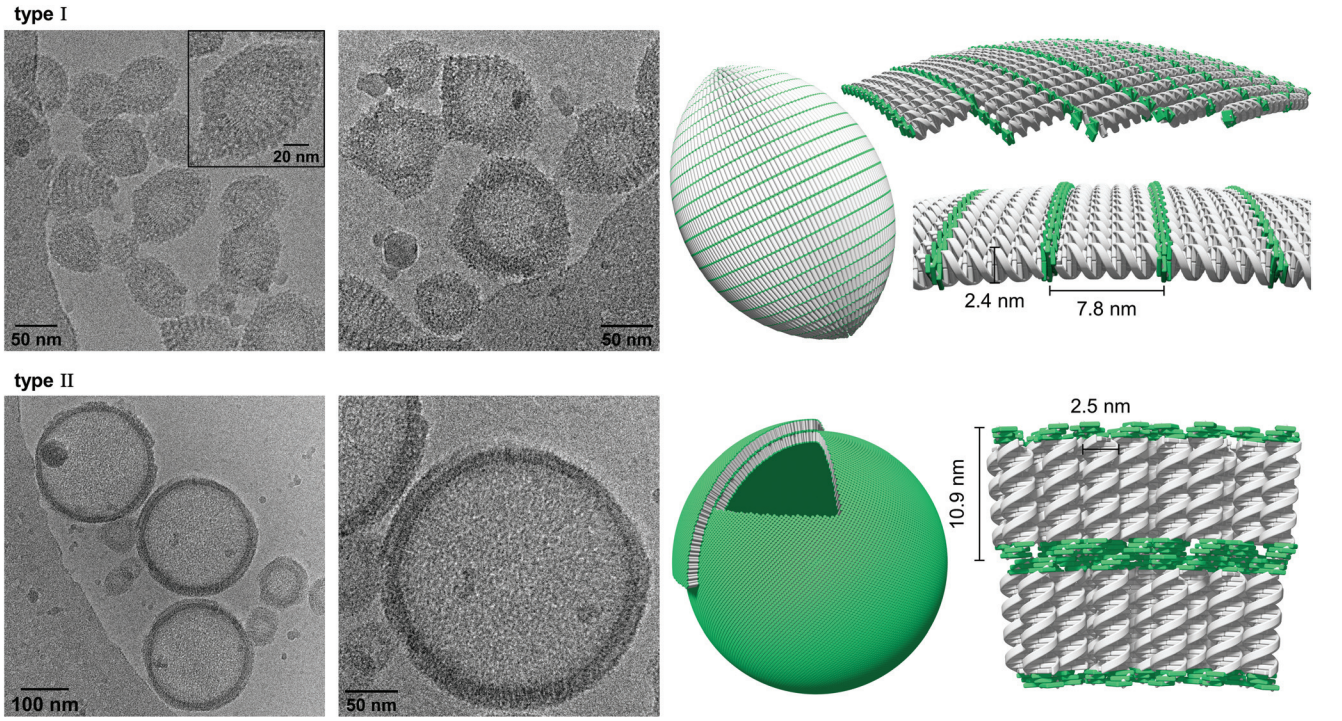

Fig. 3 Cryo-EM images and illustrations of type I vesicles (sheet-like, top) and type II vesicles (columnar, bottom). Conditions: 1 μM **A·B**, 10 mM sodium phosphate buffer pH 7.2, 0.1 mM spermine·4 HCl, 20 vol% ethanol.

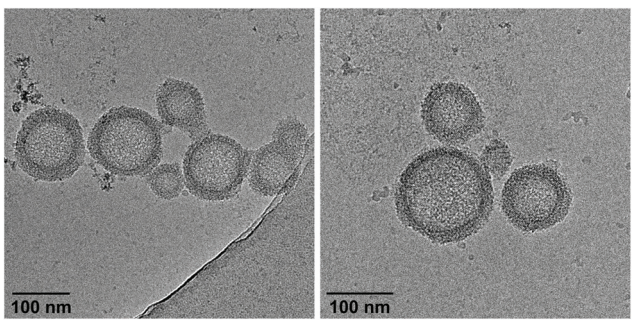

Fig. 4 Cryo-EM images of vesicles from hybrid **A·B** after removal of ethanol by dialysis. Conditions: 1 μM **A·B**, 10 mM sodium phosphate buffer pH 7.2, 0.1 mM spermine·4 HCl.

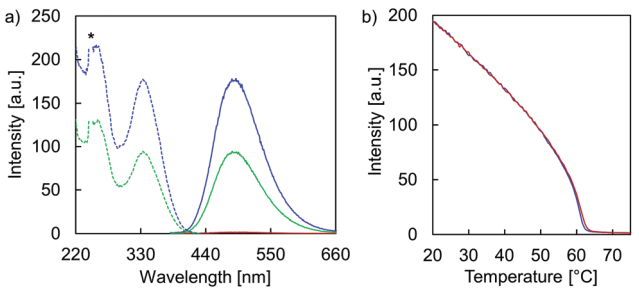

Fig. 5 (a) Fluorescence (solid line) and excitation (dotted line) spectra of **A·B** in aqueous medium at 75 °C (red), after thermally controlled assembly at 20 °C (blue), and at 20 °C after dialysis (green, <0.5 vol% ethanol). (b) Fluorescence-monitored annealing (blue) and melting (red) curves of **A·B**. Conditions: 1 μM **A·B**, 10 mM sodium phosphate buffer pH 7.2, 0.1 mM spermine·4 HCl, ethanol: 20 vol% (unless indicated otherwise), $\lambda_{ex.}$: 335 nm, $\lambda_{em.}$: 490 nm, temperature gradient: 0.5 °C min^{-1}, * indicates a second-order diffraction.

maximum of the structureless emission band is centered around 490 nm with a substantially increased Φ_{FL} (31%). The excitation spectrum confirms that fluorescence originates from the AIE-active TPE units (Fig. 5a). The mechanism of the supramolecular assembly process was examined by fluorescence monitored annealing curves (Fig. 5b). The shape of the curve is non-sigmoidal, featuring a sharp increase in fluorescence with an onset temperature of 62 °C. This strongly suggests a cooperative assembly process[47,48] of the vesicles, with a nucleation temperature around 62 °C.

DNA intercalation experiments using EthBr were performed in order to gain information on the accessibility of DNA in the formed vesicles. Taking the neighbor exclusion principle[49]

Table 1 Fluorescence quantum yields (Φ_{FL}) of **A·B** under different conditions. Φ_{FL} were determined either at 75 °C (disassembled state), at 20 °C after the assembly process (type I vesicles), or at 20 °C after dialysis (type II vesicles)

	75 °C	20 °C, after assembly process	20 °C, after dialysis
Φ_{FL} [%]	<0.75	31 ± 1	23 ± 2

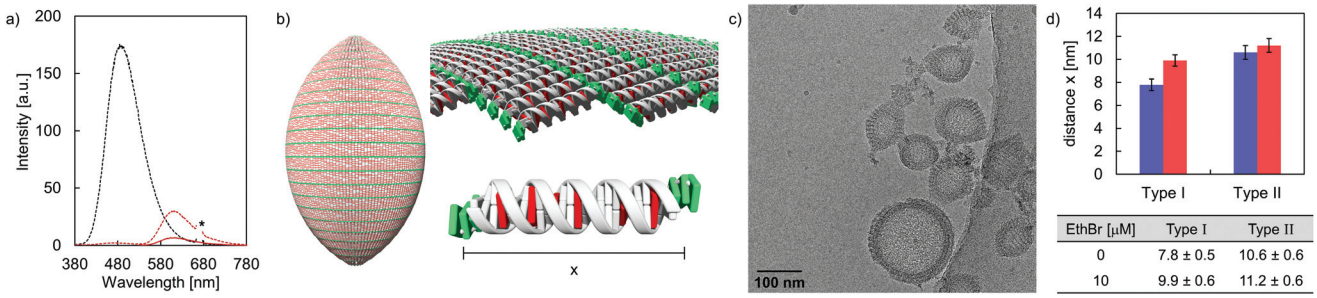

EthBr [μM]	Type I	Type II
0	7.8 ± 0.5	10.6 ± 0.6
10	9.9 ± 0.6	11.2 ± 0.6

Fig. 6 (a) Fluorescence emission spectra of vesicles assembled from duplex **A·B** in aqueous medium at 20 °C in the absence (black) and presence of 10 μM EthBr (red). Conditions: 1 μM **A·B**, 10 mM sodium phosphate buffer pH 7.2, 0.1 mM spermine·4 HCl, 20 vol% ethanol, solid line: $\lambda_{ex.}$: 520 nm, dotted line: $\lambda_{ex.}$: 335 nm. (b) Illustration of EthBr (red) intercalation. (c) Cryo-EM image in the presence of 10 μM EthBr. (d) EthBr intercalation leads to a statistically significant widening of the bands in type I vesicles.

into account, up to 10 EthBr can intercalate into the 20-mer DNA duplex **C·D** (Fig. S28, ESI†).[50] Upon intercalation, the fluorescence emission signal is enhanced, compared to the intrinsic fluorescence of free EthBr in solution (Fig. S29–S32, ESI†).[51,52] After the addition of EthBr (10 μM) to the rugby-ball-shaped type I vesicles, TPE emission is almost completely quenched upon TPE excitation (Fig. 6a). Instead, a new band centered around 610 nm, due to EthBr emission emerged, which implies excitation energy transfer from the TPE units to EthBr. Based on the relative integrated fluorescence intensities (EthBr excitation at 520 nm) between the DNA duplex **C·D** and hybrid **A·B**, it was calculated that about 6 EthBr intercalate per duplex **A·B** (Fig. 6b and Table S4, ESI†). On the other hand, only small amounts of EthBr (≤2 per DNA) may intercalate in type II vesicles, indicating that just the extended arrangement in type I vesicles enables efficient EthBr intercalation. Cryo-EM imaging supports EthBr intercalation into type I vesicles (Fig. 6c), which demonstrates a statistically significant widening of the discrete bands from originally 7.8 ± 0.5 nm to 9.9 ± 0.6 nm after the addition of EthBr (Fig. 6d). Assuming a lengthening of the helix by 3.4 Å per intercalator,[53,54] approximately 6 EthBr are intercalated per hybrid **A·B**, which is in line with the results obtained from fluorescence spectroscopy. No statistically significant extension (from 10.6 ± 0.6 nm to 11.2 ± 0.6 nm) was observed when EthBr was added to type II vesicles (Fig. S22, ESI†).

The addressability and accessibility of the vesicles was further studied by incorporation experiments of a Cy3-labelled DNA single strand **E** (Fig. 7a). Strand **E** is complementary to strand **A**. After incorporation of strand **E** into the vesicular membrane by DNA strand exchange, excitation energy transfer from the TPE donors to Cy3 acceptor is expected ($\lambda_{ex.}$: 335 nm). Doping of type I vesicles with Cy3 (1 mol% per TPE unit) was accomplished by simple addition of strand **E** to the preformed

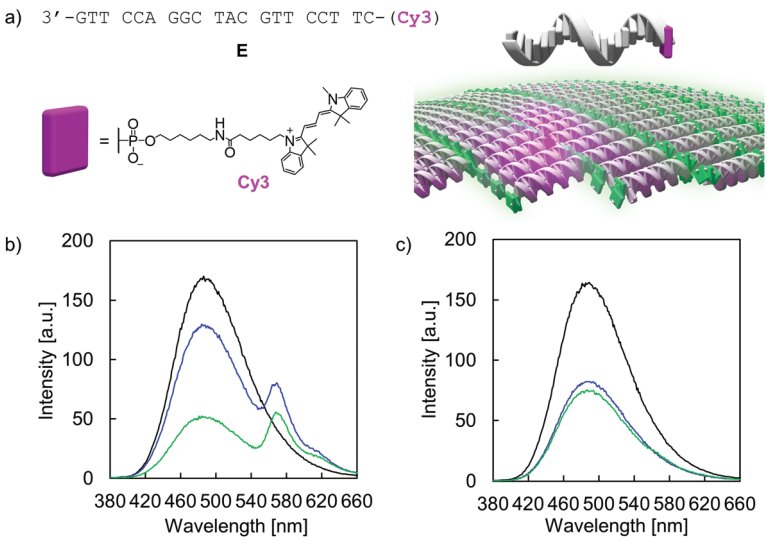

Fig. 7 (a) Sequence of the Cy3-labelled DNA single strand **E** and illustration of a Cy3-doped vesicular membrane. (b) Fluorescence emission spectra of vesicles assembled from hybrid **A·B** at 20 °C in the absence (black) and presence of 1 mol% **E**, before (blue) and after (green) dialysis. Conditions: 1 μM **A·B**, 10 mM sodium phosphate buffer pH 7.2, 0.1 mM spermine·4 HCl, $\lambda_{ex.}$: 335 nm. (c) Fluorescence emission spectra of vesicles from hybrid **A·B** (1 μM) at 20 °C in the absence of **E** before (black) and after (blue) dialysis and after dialysis in the presence of 1 mol% **E** (green), $\lambda_{ex.}$: 335 nm.

vesicles at 20 °C and waiting for 10 min before measurement. This doping process leads to a reduction of TPE emission, along with the appearance of Cy3 emission at 570 nm (Fig. 7b). Energy transfer is presumably taking place *via* a Förster resonance energy transfer (FRET) mechanism. The FRET efficiency was calculated according to integrated TPE fluorescence intensities (Fig. S36 and Table S5, ESI†). Based on this, 22 ± 4 TPE units contribute to the observed excitation energy transfer to the Cy3 acceptor in this artificial light-harvesting complex. Light-harvesting properties are maintained after dialysis, indicating that strand **E** is not removed by dialysis (Fig. 7b). Control experiments with a non-complementary, Cy3-modified DNA single strand **F** show no energy transfer and thus confirming the sequence specificity of the doping process (Fig. S38 and S39, ESI†). When strand **E** was added to type II vesicles, only marginal energy transfer was observed (Fig. 7c). Since type II vesicles are partially multi-lamellar, this observation can be explained by edge effects, *i.e.* strand exchange and incorporation of strand **E** can only take place at the exposed areas but not in the core of the compact, columnar arrangement.

Conclusions

In conclusion, the assembly of an amphiphilic DNA possessing TPE sticky ends at both sides into two different types of vesicular constructs has been demonstrated. Cryo-EM imaging reveals a regular alignment of DNA duplexes in both types of vesicular morphologies. Vesicles of type I appear as prolate ellipsoids with a diameter of 50–100 nm. The dimensions of the vesicular membrane suggest an extended arrangement of DNA duplexes that interact *via* AIE-active TPE sticky ends in the presence of spermine. Type II vesicles, on the other hand, exhibit a thicker membrane, which is compatible with a model of DNA duplexes arranged in a more compact (columnar) manner. The abundance as well as the size of type II vesicles is influenced by the solvent composition (*i.e.* ethanol content). The type of arrangement plays a crucial role for the accessibility of the DNA duplexes. Thus, only type I vesicles exhibiting the extended DNA duplex alignment are amenable to ethidium intercalation or to the incorporation of a Cy3-labelled DNA *via* strand exchange. The incorporation of acceptor chromophores into type I vesicles resulted in the formation of light-harvesting vesicular constructs. Ongoing research focuses on exploring the suitability of the presented vesicles for light-harvesting applications or as DNA-addressable nanocarriers for targeted delivery.

Author contributions

S. R. designed the project, synthesized the oligomers, performed the experiments, analyzed the data, and wrote the paper. I. I. performed cryo-EM experiments, analyzed the data, and contributed to the writing of the paper. S. M. L. designed the project, analyzed the data, created the artwork, and contributed to the writing of the paper. B. Z. designed and supervised the project and contributed to the writing of the paper. R. H. designed and supervised the project, analyzed the data, and wrote the paper.

Conflicts of interest

There are no conflicts to declare.

Acknowledgements

Financial support by the Swiss National Foundation (200020_188468 to RH and 179520 to BZ) is gratefully acknowledged. Cryo-electron microscopy was performed on equipment supported by the Microscopy Imaging Center (MIC), University of Bern, Switzerland.

References

1 U. Feldkamp and C. M. Niemeyer, *Angew. Chem., Int. Ed.*, 2006, **45**, 1856–1876.
2 N. C. Seeman, *Nature*, 2003, **421**, 427–431.
3 Y.-J. Chen, B. Groves, R. A. Muscat and G. Seelig, *Nat. Nanotechnol.*, 2015, **10**, 748–760.
4 H. Ramezani and H. Dietz, *Nat. Rev. Genet.*, 2020, **21**, 5–26.
5 P. W. K. Rothemund, *Nature*, 2006, **440**, 297–302.
6 J. R. Burns, E. Stulz and S. Howorka, *Nano Lett.*, 2013, **13**, 2351–2356.
7 R. P. Thomsen, M. G. Malle, A. H. Okholm, S. Krishnan, S. S. R. Bohr, R. S. Sørensen, O. Ries, S. Vogel, F. C. Simmel, N. S. Hatzakis and J. Kjems, *Nat. Commun.*, 2019, **10**, 5655.
8 N. C. Seeman, *DNA Cell Biol.*, 1991, **10**, 475–486.
9 E. Ban and C. R. Picu, *Biomacromolecules*, 2014, **15**, 143–149.
10 M. N. Hansen, A. M. Zhang, A. Rangnekar, K. M. Bompiani, J. D. Carter, K. V. Gothelf and T. H. LaBean, *J. Am. Chem. Soc.*, 2010, **132**, 14481–14486.
11 Y. P. Ohayon, C. Hernandez, A. R. Chandrasekaran, X. Wang, H. O. Abdallah, M. A. Jong, M. G. Mohsen, R. Sha, J. J. Birktoft, P. S. Lukeman, P. M. Chaikin, S. L. Ginell, C. Mao and N. C. Seeman, *ACS Nano*, 2019, **13**, 7957–7965.
12 D. Bhatia, S. Mehtab, R. Krishnan, S. S. Indi, A. Basu and Y. Krishnan, *Angew. Chem., Int. Ed.*, 2009, **48**, 4134–4137.
13 M. Vybornyi, Y. Vyborna and R. Häner, *Chem. Soc. Rev.*, 2019, **48**, 4347–4360.
14 S. P. W. Wijnands, E. W. Meijer and M. Merkx, *Bioconjugate Chem.*, 2019, **30**, 1905–1914.
15 M. Madsen and K. V. Gothelf, *Chem. Rev.*, 2019, **119**, 6384–6458.
16 C. Gong, S. Sun, Y. Zhang, L. Sun, Z. Su, A. Wu and G. Wei, *Nanoscale*, 2019, **11**, 4147–4182.

17 J.-F. Lutz, *ACS Macro Lett.*, 2020, **9**, 185–189.
18 C. J. Serpell, M. Barłóg, K. Basu, J. F. Fakhoury, H. S. Bazzi and H. F. Sleiman, *Mater. Horiz.*, 2014, **1**, 348–354.
19 E. M. Estirado, M. A. A. Garcia, J. Schill and L. Brunsveld, *J. Am. Chem. Soc.*, 2019, **141**, 18030–18037.
20 P. Ensslen, S. Gärtner, K. Glaser, A. Colsmann and H.-A. Wagenknecht, *Angew. Chem., Int. Ed.*, 2016, **55**, 1904–1908.
21 X. Wang, R. Sha, M. Kristiansen, C. Hernandez, Y. Hao, C. Mao, J. W. Canary and N. C. Seeman, *Angew. Chem., Int. Ed.*, 2017, **56**, 6445–6448.
22 H. Bui, S. A. Díaz, J. Fontana, M. Chiriboga, R. Veneziano and I. L. Medintz, *Adv. Opt. Mater.*, 2019, **7**, 1900562.
23 M. Kownacki, S. M. Langenegger, S.-X. Liu and R. Häner, *Angew. Chem., Int. Ed.*, 2019, **58**, 751–755.
24 B. L. Li, R. Li, H. L. Zou, K. Ariga, N. B. Li and D. T. Leong, *Mater. Horiz.*, 2020, **7**, 455–469.
25 D. Bousmail, L. Amrein, J. J. Fakhoury, H. H. Fakih, J. C. C. Hsu, L. Panasci and H. F. Sleiman, *Chem. Sci.*, 2017, **8**, 6218–6229.
26 C.-H. Lu and I. Willner, *Angew. Chem., Int. Ed.*, 2015, **54**, 12212–12235.
27 Z.-Y. Wang, C.-P. Zhang and C.-Y. Zhang, *Chem. Commun.*, 2020, **56**, 2119–2122.
28 B. Shin, W.-K. Kim, S. Yoon and J. Lee, *Sens. Actuators, B*, 2020, **305**, 127471.
29 S. R. Bandara, T. G. Molley, H. Kim, P. A. Bharath, K. A. Kilian and C. Leal, *Mater. Horiz.*, 2020, **7**, 125–134.
30 Y. H. Roh, J. B. Lee, P. Kiatwuthinon, M. R. Hartman, J. J. Cha, S. H. Um, D. A. Muller and D. Luo, *Small*, 2011, **7**, 74–78.
31 A. Patwa, A. Gissot, I. Bestel and P. Barthélémy, *Chem. Soc. Rev.*, 2011, **40**, 5844–5854.
32 N. Dave and J. Liu, *ACS Nano*, 2011, **5**, 1304–1312.
33 P. M. G. Löffler, O. Ries, A. Rabe, A. H. Okholm, R. P. Thomsen, J. Kjems and S. Vogel, *Angew. Chem., Int. Ed.*, 2017, **56**, 13228–13231.
34 S. Matoori and J.-C. Leroux, *Mater. Horiz.*, 2020, **7**, 1297–1309.
35 Y. Kamiya, Y. Yamada, T. Muro, K. Matsuura and H. Asanuma, *ChemMedChem*, 2017, **12**, 2016–2021.
36 C. D. Bösch, J. Jevric, N. Bürki, M. Probst, S. M. Langenegger and R. Häner, *Bioconjugate Chem.*, 2018, **29**, 1505–1509.
37 J. Luo, Z. Xie, J. W. Y. Lam, L. Cheng, H. Chen, C. Qiu, H. S. Kwok, X. Zhan, Y. Liu, D. Zhu and B. Z. Tang, *Chem. Commun.*, 2001, 1740–1741.
38 J. Mei, N. L. C. Leung, R. T. K. Kwok, J. W. Y. Lam and B. Z. Tang, *Chem. Rev.*, 2015, **115**, 11718–11940.
39 Y. Chen, J. W. Y. Lam, R. T. K. Kwok, B. Liu and B. Z. Tang, *Mater. Horiz.*, 2019, **6**, 428–433.
40 Y. Zhang, Y. Wang, J. Wang and X.-J. Liang, *Mater. Horiz.*, 2018, **5**, 799–812.
41 J. Dubochet, M. Adrian, J.-J. Chang, J.-C. Homo, J. Lepault, A. W. McDowall and P. Schultz, *Q. Rev. Biophys.*, 1988, **21**, 129–228.
42 M. Adrian, B. ten Heggeler-Bordier, W. Wahli, A. Z. Stasiak, A. Stasiak and J. Dubochet, *EMBO J.*, 1990, **9**, 4551–4554.
43 S. Li, S. M. Langenegger and R. Häner, *Chem. Commun.*, 2013, **49**, 5835–5837.
44 C. T. Rueden, J. Schindelin, M. C. Hiner, B. E. DeZonia, A. E. Walter, E. T. Arena and K. W. Eliceiri, *BMC Bioinf.*, 2017, **18**, 529.
45 J. Schindelin, I. Arganda-Carreras, E. Frise, V. Kaynig, M. Longair, T. Pietzsch, S. Preibisch, C. Rueden, S. Saalfeld, B. Schmid, J.-Y. Tinevez, D. J. White, V. Hartenstein, K. Eliceiri, P. Tomancak and A. Cardona, *Nat. Methods*, 2012, **9**, 676–682.
46 M. Linkert, C. T. Rueden, C. Allan, J.-M. Burel, W. Moore, A. Patterson, B. Loranger, J. Moore, C. Neves, D. MacDonald, A. Tarkowska, C. Sticco, E. Hill, M. Rossner, K. W. Eliceiri and J. R. Swedlow, *J. Cell Biol.*, 2010, **189**, 777–782.
47 D. Zhao and J. S. Moore, *Org. Biomol. Chem.*, 2003, **1**, 3471–3491.
48 P. A. Korevaar, S. J. George, A. J. Markvoort, M. M. J. Smulders, P. A. J. Hilbers, A. P. H. J. Schenning, T. F. A. De Greef and E. W. Meijer, *Nature*, 2012, **481**, 492–496.
49 J. Cairns, *Cold Spring Harbor Symp. Quant. Biol.*, 1962, **27**, 311–318.
50 M. J. Waring, *J. Mol. Biol.*, 1965, **13**, 269–282.
51 J. B. Lepecq and C. Paoletti, *J. Mol. Biol.*, 1967, **27**, 87–106.
52 J. Olmsted and D. R. Kearns, *Biochemistry*, 1977, **16**, 3647–3654.
53 L. S. Lerman, *J. Mol. Biol.*, 1961, **3**, 18–30.
54 G. M. Blackburn, M. J. Gait, D. Loakes and D. M. Williams, *Nucleic Acids in Chemistry and Biology*, Royal Society of Chemistry, Cambridge, 2006.